Thomas–Fermi–Dirac–von Weizsäcker hydrodynamics in parabolic wells

E. Zaremba and H. C. Tso

Department of Physics, Queen's University, Kingston, Ontario, Canada K7L 3N6

(Received 2 September 1993)

A hydrodynamic description of the collective excitations of an inhomogeneous electronic system is developed on the basis of the Thomas–Fermi–Dirac–von Weizsäcker approximation to the equilibrium ground state. This approximation allows one to define realistic equilibrium densities which are then used to obtain a consistent description of the dynamical behavior. An application to a parabolically confined electron gas is presented and the magnetoplasmon modes are obtained from a solution of the linearized hydrodynamic equations. The wave-vector dispersion of the modes is determined, as well as the detailed dependence on the orientation of the applied magnetic field. The power absorption in the long-wavelength limit is also calculated to illustrate the center-of-mass mode excitations probed by transmission experiments.

I. INTRODUCTION

A hydrodynamic description of electron dynamics in matter goes back to the early work of Bloch[1] and has since been applied to a wide range of problems.[2-4] Within this approach, the many-electron system is represented as a charged fluid whose dynamics is described in terms of a density and velocity field. Its main appeal is its relative simplicity. Although the approach is usually introduced heuristically, with no presumption of theoretical rigor, it can be viewed as an approximate extension[5] of density-functional theory[6] to the dynamic regime. Considering the complexity of treating dynamics with formal many-body techniques,[7,8] it is clearly of considerable interest to develop methods which are easier to implement and, at the same time, trustworthy in their qualitative predictions.

The application to homogeneous systems is straightforward and in the case of an electron gas yields the expected collective plasmon excitation. This mode is sustained by electron-electron interactions which are accounted for in terms of a self-consistent polarization field generated by the density fluctuation. The internal properties of the electron gas are also important in that they distinguish, for example, between degenerate and nondegenerate systems. Some of this information can be included by means of a stress tensor, usually approximated as an isotropic pressure which, in the case of plasmons, leads to a wave-vector dispersion of the plasmon frequency. Although the collective aspects are well represented, the hydrodynamic approach has the one limitation of failing to represent the internal degrees of freedom which manifest themselves as single-particle excitations. However, this limitation is not severe, and some of these effects can be included by introducing a phenomenological damping or relaxation rate which has the effect of giving the collective mode a finite lifetime.

Of more interest, however, are applications to inhomogeneous systems.[4,9] Hydrodynamic theory has been used extensively in the study of the electromagnetic response of metal surfaces, both in the linear[10-12] and nonlinear

regimes.[13,14] In the crudest approximation, the metal is represented as a homogeneous material bounded by a surface plane at which the properties of the metal change discontinuously from the interior of the metal to the exterior vacuum region. This approximation is reasonable when the response of the material is represented by a local, frequency-dependent dielectric function, but it leads to difficulties when attempts are made to include the nonlocality of the response behavior via hydrodynamics. Since the hydrodynamic equations are partial differential equations, their solution depends on specifying a set of boundary conditions at the surface of the metal. Apart from the usual electromagnetic boundary conditions, additional boundary conditions (ABC's) are needed and are usually specified by considering the flux of conserved quantities (mass, momentum, and energy) at the surface.[4] These ABC's are not generally compatible, so that the particular choice made is to some extent arbitrary. The fact that physical predictions are sensitive to the boundary conditions[12] has led to justified concerns about the usefulness of the hydrodynamic model in providing a realistic description of surface dynamics.

Attempts to improve upon the results by using more realistic equilibrium surface densities, in particular densities which vary continuously from the interior of the metal into the vacuum region, have also met with limited success.[12] For example, continuous surface densities lead to a proliferation of surface multipole modes which do not bear an obvious correspondence to experimental observation. Similar unphysical behavior is found in studies of collective modes in modulated two-dimensional electron gases.[15] In the limit of strong modulation, the two-dimensional gas segregates into an array of one-dimensional wires which are separated by regions of near-zero density. It is found[15] that the plasmon modes in this limit are associated with density fluctuations which appear to be localized in the low-density regions, reminiscent of the spurious surface multipole modes at a metallic surface. The more sophisticated calculations based on the random-phase approximation (RPA) do not support this kind of behavior.[16] One is left with the im-

pression that the application of hydrodynamic theory to inhomogeneous systems is at best subject to considerable uncertainty.

In this paper we wish to demonstrate that the hydrodynamic theory for inhomogeneous systems can be salvaged when suitably generalized to properly account for mechanical equilibrium. Failure to do so introduces spurious forces which corrupt the dynamical analysis. The important point is that an inhomogeneous system is the ground state of a collection of electrons in some external confining potential, and in principle must be determined by a quantum-mechanical electronic structure calculation. Density-functional theory at the level of the local-density approximation is the most commonly used method for establishing these properties. However if Kohn-Sham theory,[17] a wave mechanical approach, is adopted, response calculations must be performed at the level of time-dependent density-functional theory[18,19] which necessitates the calculation of electronic response functions.[20,19,21] It is precisely this aspect that a hydrodynamic approach attempts to avoid. This objective can be realized by using an energy functional, such as Thomas[22]–Fermi[23]–von Weizsäcker[24] (TFW), which is exclusively a functional of the density.[25] Although less accurate than the full quantum-mechanical calculation, this approximation has the virtue of incorporating the effects of the quantum-mechanical kinetic energy, and leads to ground-state densities which are smooth and continuous. This latter property is especially advantageous since it allows one to dispense with ABC's.

As an application of our generalized hydrodynamic theory, we investigate the collective modes in a parabolically confined electron gas. This situation is very similar to that of a thin metallic film in which the electrons are confined by a slab of positive charge. However, in the parabolically confined system, achieved experimentally in semiconductor heterostructures,[26,27] the external potential is purely parabolic for all positions in the confining direction. Recently, this system has been investigated in considerable detail by Dempsey and Halperin[28] (hereafter referred to as DH) using a hydrodynamic theory based on a modified form of the Thomas-Fermi (TF) approximation. Instead of using the true nonlinear TF pressure, they introduce a linearized approximation whereby the pressure is of the form $p \propto (n - n_c)$. The parameter n_c dictates the form of the equilibrium density profile, and for the most part they choose a value which leads to a constant density slab. Although other values of n_c admit physically more realistic charge distributions, DH caution that the associated collective excitations need not be more reliable. Here we show that when TF is extended to include the von Weizsäcker correction to the kinetic energy, realistic equilibrium densities can be generated, and that the oscillations about equilibrium are not subject to the pathologies previously encountered when continuous densities were used either with[12] or without[15] the TF pressure.

An outline of our paper follows. In Sec. II we describe the equilibrium properties as provided by the TFW approximation with the additional inclusion of a local exchange energy [Thomas–Fermi–Dirac–von Weizsäcker

(TFDW)]. The hydrodynamic equations used to represent the dynamics of the electron fluid are introduced, and the internal forces arising from the TFDW approximation are defined. As an application, in Sec. III we consider a parabolically confined electron gas. A solution of the linearized problem is developed which makes use of a particularly convenient basis of functions defined by the TFDW equilibrium state. The magnetoplasmon waves in this geometry are studied for various orientations of an externally applied magnetic field, and as a function of the propagation wave vector. We also show that the frequency of the center-of-mass mode complies with the generalization of Kohn's theorem.[29] In Sec. IV we derive expressions for the power absorption, which is typically measured in infrared transmission experiments and show, in the case of parabolic confinement, that only the center-of-mass modes are excited. Finally, in Sec. V we present our concluding remarks.

II. EQUILIBRIUM AND HYDRODYNAMIC EQUATIONS

We define the equilibrium electronic properties in terms of the following energy functional:

$$E[n] = \int d\mathbf{r} \left[C_1 n^{5/3}(\mathbf{r}) + C_2 \frac{[\nabla n(\mathbf{r})]^2}{n(\mathbf{r})} - C_x n(\mathbf{r})^{4/3} \right]$$
$$+ \frac{1}{2} \int d\mathbf{r} \int d\mathbf{r}' \frac{n(\mathbf{r})n(\mathbf{r}')}{|\mathbf{r}-\mathbf{r}'|} + \int d\mathbf{r}\, v_{\text{ext}}(\mathbf{r})n(\mathbf{r}) , \quad (1)$$

where $n(\mathbf{r})$ is the electronic density. The first two terms are the Thomas-Fermi and von Weizsäcker kinetic-energy functionals, respectively, with coefficients

$$C_1 = \tfrac{3}{10}(3\pi^2)^{2/3}, \quad C_2 = \frac{\lambda_w}{8} , \quad (2)$$

where we use atomic units $(e^2/\epsilon = m^* = \hbar = 1)$ throughout. The parameter λ_w has the value 1 in the original von Weizsäcker formulation,[24] but a value closer to 0.25 provides a better representation of a Kohn-Sham calculation.[30-32] The third term is the Dirac (or local) exchange energy[6,25] with coefficient

$$C_x = \frac{3}{4}\left[\frac{3}{\pi}\right]^{1/3} , \quad (3)$$

the fourth term is the classical electrostatic self-energy, and the final term is the interaction of the electrons with whatever external potential is present. This energy functional could be augmented with an additional correlation energy,[32] but this plays a relatively minor role and we have chosen to neglect it for simplicity.

The ground-state properties are obtained by finding the variational minimum of Eq. (1) subject to the constraint that the total number of electrons is fixed. Introducing the Lagrange parameter μ, the equilibrium density is determined by the Euler equation

$$\frac{\delta E[n]}{\delta n(\mathbf{r})} - \mu = 0 , \quad (4)$$

which leads to

$$-2C_2\frac{\nabla^2 n(\mathbf{r})}{n(\mathbf{r})}+C_2\left[\frac{\nabla n(\mathbf{r})}{n(\mathbf{r})}\right]^2+\tfrac{5}{3}C_1 n^{2/3}(\mathbf{r})$$
$$-\tfrac{4}{3}C_x n^{1/3}(\mathbf{r})+\phi(\mathbf{r})+v_{\text{ext}}(\mathbf{r})-\mu=0 \ . \quad (5)$$

Here, $\phi(\mathbf{r})$ is the electrostatic potential arising from the electronic density $n(\mathbf{r})$ and is the solution of Poisson's equation:

$$\nabla^2\phi(\mathbf{r})=-4\pi n(\mathbf{r}) \ . \quad (6)$$

The Lagrange multiplier μ is the chemical potential of the many-electron system, and is chosen to ensure that the total number of electrons is some specified value N.

It is convenient to introduce a wave function according to the definition $n(\mathbf{r})=\psi^2(\mathbf{r})$. In terms of this variable, the Euler equation takes the form of a Schrödinger-like equation

$$-\frac{\lambda_w}{2}\nabla^2\psi(\mathbf{r})+v_{\text{eff}}(\mathbf{r})\psi(\mathbf{r})=\mu\psi(\mathbf{r}) \ , \quad (7)$$

where the effective potential is defined by

$$v_{\text{eff}}(\mathbf{r})=\tfrac{5}{3}C_1\psi^{4/3}(\mathbf{r})-\tfrac{4}{3}C_x\psi^{2/3}(\mathbf{r})+\phi(\mathbf{r})+v_{\text{ext}}(\mathbf{r}) \ . \quad (8)$$

It should be noted that in contrast to the usual Kohn-Sham (KS) effective potential, the potential defined here has an additional kinetic-energy contribution coming from the TF term. The parameter λ_w^{-1} plays the role of a mass, which is not to be confused with the actual effective mass m^* of the electrons. The smaller the value of λ_w, the heavier is the quantum particle and the closer is the solution to the semiclassical Thomas-Fermi-Dirac (TFD) result. Equation (7) is a nonlinear equation in the wave function which must be solved self-consistently. In doing so, we must impose the normalization

$$\int d\mathbf{r}\,\psi^2(\mathbf{r})=N \ . \quad (9)$$

The required solution to Eq. (7) is of course the ground-state wave function, and the ground-state energy is then the chemical potential.

The equilibrium condition given by the Euler equation can also be interpreted as the balance of all classical forces acting on each fluid element, namely,

$$\mathbf{F}_0(\mathbf{r})\equiv-\nabla\left[\frac{\delta E[n]}{\delta n(\mathbf{r})}\right]_{n_0}=0 \ . \quad (10)$$

This observation leads naturally to the definition of the force in dynamic situations as

$$\mathbf{F}(\mathbf{r},t)=-\nabla\left[v_{\text{eff}}(\mathbf{r},t)-\frac{\lambda_w}{2}\frac{\nabla^2\psi(\mathbf{r},t)}{\psi(\mathbf{r},t)}\right] \ , \quad (11)$$

where the time-dependent wave function is again defined by $n(\mathbf{r},t)=\psi^2(\mathbf{r},t)$. v_{eff} includes the internal TF pressure and Coulomb-derived potentials, while the last term contributes what can be called the von Weizsäcker force.

The dynamics of $\psi(\mathbf{r},t)$ of course is not prescribed by a time-dependent Schrödinger equation, but is assumed to be determined by a set of hydrodynamic equations governing the evolution of the density. These we take to

be the continuity equation

$$\frac{\partial n}{\partial t}+\nabla\cdot(n\mathbf{v})=0 \quad (12)$$

and the momentum equation

$$m^*n\left[\frac{\partial\mathbf{v}}{\partial t}+\mathbf{v}\cdot\nabla\mathbf{v}\right]=n\mathbf{F}-en\frac{\mathbf{v}}{c}\times\mathbf{B} \ , \quad (13)$$

where $\mathbf{F}$ includes the internal forces from Eq. (11) together with any additional externally imposed forces. We also include separately a magnetic force which is due to a uniform external magnetic field. The equilibrium situation has $\mathbf{v}=0$, and Eq. (13) reduces to Eq. (10). Assuming small deviations from equilibrium, we linearize the equations to obtain

$$\frac{\partial\delta n}{\partial t}+\nabla\cdot(n_0\mathbf{v})=0 \quad (14)$$

and

$$m^*n_0\frac{\partial\mathbf{v}}{\partial t}=n_0\delta\mathbf{F}-en_0\frac{\mathbf{v}}{c}\times\mathbf{B} \ , \quad (15)$$

where the fluctuating force is given by

$$\delta\mathbf{F}=-\nabla\left[\delta v_{\text{eff}}-\frac{\lambda_w}{2\psi_0}\nabla^2\delta\psi+\frac{\lambda_w}{2}\frac{\nabla^2\psi_0}{\psi_0^2}\delta\psi\right] \ . \quad (16)$$

Here, ψ_0 is the ground-state wave function and δv_{eff} is the variation of Eq. (8). The density fluctuation is related to $\delta\psi$ by $\delta n=2\psi_0\delta\psi$.

We seek harmonic solutions of the form $\mathbf{v}\propto e^{-i\omega t}$. Equation (15) can then be solved easily for $\mathbf{v}$ regardless of the explicit form of $\delta\mathbf{F}$. We find

$$-i\omega(\omega^2-\omega_c^2)m^*\mathbf{v}=\omega^2\delta\mathbf{F}+i\omega\vec{\omega}_c\times\delta\mathbf{F}-\vec{\omega}_c(\vec{\omega}_c\cdot\delta\mathbf{F}) \ , \quad (17)$$

where we have introduced the cyclotron frequency vector $\vec{\omega}_c=e\mathbf{B}/m^*c$. If $\delta\mathbf{F}$ simply corresponded to a local electric field, Eq. (17) would define a local, frequency-dependent conductivity tensor. A local relationship between the current and the driving forces is a general feature of the hydrodynamic description, whereas the nonlocality enters through the connection between the forces and the density fluctuation.

Equations (14)–(16) are generally applicable, but to proceed with the solution of the dynamics, we must first specify the nature of the physical system.

III. PARABOLIC WELLS

We specialize to the case in which the electronic system is translationally invariant in the x and y directions, and confined by a harmonic potential $V(z)=\tfrac{1}{2}kz^2$ in the z direction. Because of its relative simplicity, this particular geometry is ideally suited to illustrating the general approach. In addition, a comparison can be made with results that have already appeared[28] using cruder approximations.

Before discussing the ground-state solution of Eq. (7), we first note that the purely classical approximation in

which only electrostatic interactions are included $(C_1=C_2=C_x=0)$ corresponds to a bounded, constant density slab of electrons. This density profile is also obtained in the modified Thomas-Fermi (MTF) approximation of DH. The three-dimensional electron density n_{3D} is determined by the potential curvature according to the condition $\omega_p^2=k/m^*$, where ω_p is the three-dimensional plasma frequency $\omega_p=(4\pi n_{3D}e^2/m^*\epsilon)^{1/2}$. We have in mind an application to parabolic wells in GaAs for which $m^*=0.067m_e$ and the background dielectric constant is $\epsilon=13.0$. For this situation the effective Bohr radius is $a_0^*=103$ Å, and the effective Rydberg of energy is $Ry^*=e^2/2\epsilon a_0^*=5.4$ meV. The width W of the uniform slab is determined by $W=n_{2D}/n_{3D}$, where n_{2D} is the 2D areal density.

The discontinuous density profile of the classical or MTF approximations is eliminated when the fully nonlinear TF or TFD approximations are used. The equilibrium density then goes to zero at a definite finite distance from the center of the slab.[33] When the von Weizsäcker kinetic energy is included, the density is further modified and now exhibits an asymptotic decay to zero which is governed by both the TF screening length and the λ_w parameter. In our calculations, except when specified otherwise, we use $\lambda_w=0.25$, which was previously found to give a reasonable description of jellium surface densities and other physical properties.[32] The solution of Eq. (7) can be obtained straightforwardly by iteration, and equilibrium density profiles are shown in Fig. 1 for a few typical cases. In Fig. 2(a) we also show the effect of changing λ_w from 0.25 to 1.0; as expected, the decay length of the density at the edge of the slab increases with increasing λ_w. Similarly, in Fig. 2(b) we show the effect of eliminating the exchange interaction with $\lambda_w=0.25$. The density exhibits a more pronounced overshoot when exchange is included, indicating the importance of the Dirac exchange energy. Comparison with KS calculations[34,35] shows that the TFDW densities are qualitatively similar although they are somewhat smoother and exhibit less oscillatory structure. This difference is partly due to the fact that the KS densities are composed of a superposition of several subband states which have an increasing
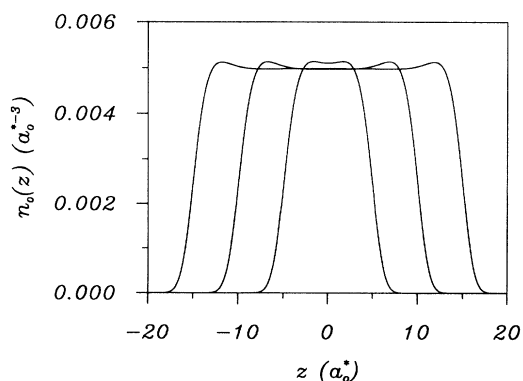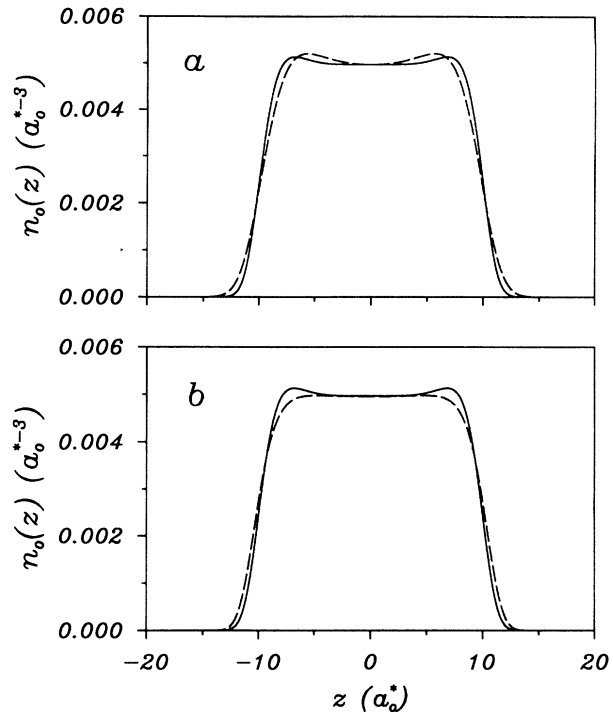

FIG. 2. (a) Equilibrium profiles for $n_{2D}=0.1(a_0^*)^{-2}$ with $\lambda_w=0.25$ (solid line) and $\lambda_w=1.0$ (dashed line). (b) As in (a), but for $\lambda_w=0.25$ with (solid line) and without (dashed line) exchange.

number of nodes with increasing energy. The TFDW wave function, on the other hand, is nodeless. Furthermore, in order to acquire the flat-topped behavior for the wider wells, the ground-state eigenvalue must lie very close to the bottom of the self-consistent potential. An example of this is shown in Fig. 3.

We now obtain wavelike solutions to Eqs. (14)–(17) for the geometry illustrated in Fig. 4. The propagation vector q is taken to be in the x direction, while the applied

FIG. 1. Equilibrium density profiles for a parabolic potential with $\omega_p=0.5$ Ry*. The curves with increasing width correspond to $n_{2D}=0.05, 0.1$, and $0.15(a_0^*)^{-2}$, respectively.
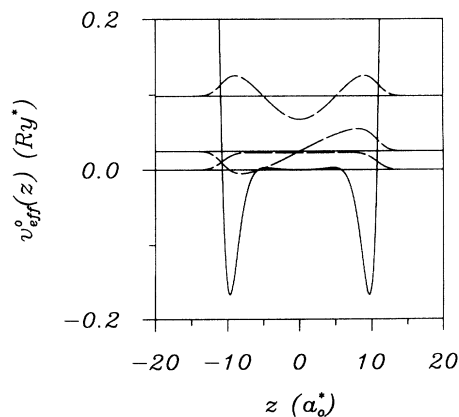

FIG. 3. Self-consistent potential for $n_{2D}=0.1(a_0^*)^{-2}$ and $\lambda_w=0.25$, including exchange (solid line). Also shown as dashed lines are the lowest three TFDW wave functions [see Eq. (23)]. The horizontal lines denote the corresponding eigenvalues with the ground-state eigenvalue set to zero.
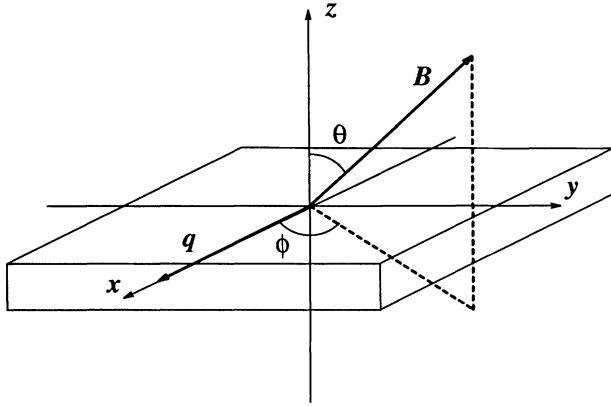
FIG. 4. Geometry and coordinate system for the parabolic well with confinement in the z direction. The wave vector q is chosen to lie along the x axis, and the magnetic-field orientation is specified by the angles θ and ϕ.

magnetic field has an arbitrary orientation. All fluctuating variables are assumed proportional to $e^{i(qx-\omega t)}$, with amplitudes that are functions of z. For example, the fluctuating part of the wave function is

$$\delta\psi = u(z)e^{i(qx-\omega t)} \ . \tag{18}$$

In this situation, the continuity equation takes the form

$$-i\omega\delta n + in_0\mathbf{q\cdot v} + \frac{d}{dz}(n_0 v_z)=0 \ , \tag{19}$$

where, from now on, we display only the z-dependent amplitudes, and the fluctuating force is

$$\delta\mathbf{F} = -i\mathbf{q}f - \frac{df}{dz}\hat{z} \ , \tag{20}$$

with

$$f = \delta v_{\text{eff}} + \frac{1}{\psi_0}(\hat{h} + \tfrac{1}{2}\lambda_w q^2)u \ . \tag{21}$$

Here, we have defined the Hamiltonian operator

$$\hat{h} = -\frac{\lambda_w}{2}\frac{d^2}{dz^2} + v_{\text{eff}}^0 - \mu \ , \tag{22}$$

which defines the ground-state wave function. This is a Hermitian operator with orthonormal eigenfunctions defined by

$$\hat{h}\varphi_i = \mu_i\varphi_i \ . \tag{23}$$

The lowest-energy eigenfunction is proportional to ψ_0 and, by construction, has a zero eigenvalue. As we shall see, this basis is ideally suited to obtaining a solution of the hydrodynamic equations. A few of the excited states are illustrated in Fig. 3.

Substituting Eq. (17) for the velocity into the continuity equation, and using the form of $\delta\mathbf{F}$ in Eq. (20), we find that the density fluctuation satisfies the equation (with $m^*=1$)

$$\omega^2(\omega^2-\omega_c^2)\delta n$$

$$= [\omega^2 q^2 - (\vec{\omega}_c\cdot\mathbf{q})^2]n_0 f + i\alpha n_0\frac{df}{dz} + i\alpha^*\frac{d}{dz}(n_0 f)$$

$$-(\omega^2-\omega_{cz}^2)\frac{d}{dz}\left[n_0\frac{df}{dz}\right] \ , \tag{24}$$

where

$$\alpha(\mathbf{q},\omega) = \alpha_1(\mathbf{q},\omega) + i\alpha_2(\mathbf{q},\omega)$$

$$\equiv \omega_{cz}(\mathbf{q}\cdot\vec{\omega}_c) - i\omega\hat{z}\cdot(\mathbf{q}\times\vec{\omega}_c) \ . \tag{25}$$

The expression for f in Eq. (21) shows that Eq. (24) contains derivatives of the density up to fourth order. In addition, δv_{eff} includes the induced electric potential so that Eq. (24) is actually an integrodifferential equation for δn. By making use of Poisson's equation, the density fluctuation can be eliminated in favor of the potential fluctuations, but at the cost of generating a sixth-order differential equation. This equation is exceedingly complex, with coefficients which are involved functions of $n_0(z)$ and its derivatives. A direct numerical solution is therefore prohibitive.

Fortunately, a fairly simple and straightforward procedure is available whereby one solves for the fluctuating part of the wave function u, related to δn by $\delta n = 2\psi_0 u$. This function is expanded in the form

$$u = \sum_i c_i\varphi_i \ , \tag{26}$$

where φ_i are the basis functions in Eq. (23). Substituting this expression in Eq. (24), dividing by $2\psi_0$, and projecting out the ith component using the orthonormality of the basis functions, we obtain

$$\omega^2(\omega^2-\omega_c^2)c_i = \frac{1}{2}\left[\omega^2 q^2 - (\vec{\omega}_c\cdot\mathbf{q})^2 + \frac{2\mu_i}{\lambda_w}(\omega^2-\omega_{cz}^2)\right]I_1$$

$$-i\alpha_1 I_2 + \alpha_2 I_3 \ . \tag{27}$$

In arriving at this result we have integrated by parts all terms involving a derivative of f in order to generate the three integrals

$$I_1 = \int dz\ \varphi_i\psi_0 f \ , \tag{28}$$

$$I_2 = \int dz\frac{d\varphi_i}{dz}\psi_0 f \ , \tag{29}$$

and

$$I_3 = \int dz\ \varphi_i\frac{d\psi_0}{dz}f \ . \tag{30}$$

Equation (27) is finally reduced to a matrix problem by substituting the expression for f into these integrals, and again using the expansion of u. For example,

$$I_1 = \int dz\ \varphi_i\psi_0 f = \sum_j [M_{ij}(q) + (\mu_i + \tfrac{1}{2}\lambda_w q^2)\delta_{ij}]c_j$$

$$\equiv \sum_j \tilde{M}_{ij}(q)c_j \ . \tag{31}$$

The M_{ij} matrix has three contributions: (i) the TF kinet-

ic term

$$M_{ij}^K = \frac{20}{9} C_1 \int dz \, \varphi_i \psi_0^{4/3} \varphi_j \ ,$$ (32)

(ii) the exchange term

$$M_{ij}^X = -\frac{8}{9} C_x \int dz \, \varphi_i \psi_0^{2/3} \varphi_j \ ,$$ (33)

and (iii) the Hartree or Coulomb term

$$M_{ij}^H(q) = \frac{4\pi}{q} \int dz \int dz' \varphi_i(z)\psi_0(z)$$

$$\times e^{-q|z-z'|} \varphi_j(z')\psi_0(z') \ .$$ (34)

The first two terms are q independent, in contrast to the Hartree term which is proportional to a form factor typical of screening problems in two-dimensional electron gases.[36]

The other two integrals can be evaluated similarly and lead to analogous matrices which, however, have a less symmetrical form. We will not display these here explicitly but simply write

$$I_2 = \sum_j N_{ij}(q)c_j$$ (35)

and

$$I_3 = \sum_j O_{ij}(q)c_j \ .$$ (36)

Equation (27) can now be written as

$$\omega^2(\omega^2 - \omega_c^2)c_i = \frac{1}{2}\left[\omega^2 q^2 - (\vec{\omega}_c \cdot \mathbf{q})^2 + \frac{2\mu_i}{\lambda_w}(\omega^2 - \omega_{cz}^2)\right]$$

$$\times \sum_j \tilde{M}_{ij}(q)c_j$$

$$-i\alpha_1 \sum_j N_{ij}(q)c_j + \alpha_2 \sum_j O_{ij}(q)c_j \ .$$ (37)

This equation determines the eigenfrequencies and corresponding eigenvectors of the collective modes for the most general situation we shall address. Before doing so, however, it is useful to reexpress Eq. (37) in an alternate form which facilitates a general discussion of the mode eigenvalue problem.

Rather than focusing on the density fluctuation δn, or equivalently $\delta\psi$, we consider the potential fluctuations $\psi_0 f$. This function has the expansion

$$\psi_0 f = \sum_i f_i \phi_i \ ,$$ (38)

and from Eq. (31) we see that

$$f_i = \sum_j \tilde{M}_{ij} c_j \ .$$ (39)

Equation (27) can then be expressed as

$$\omega^2(\omega^2 - \omega_c^2) \sum_j \tilde{M}_{ij}^{-1} f_j$$

$$= \frac{1}{2}\left[\omega^2 q^2 - (\vec{\omega}_c \cdot \mathbf{q})^2 + \frac{2\mu_i}{\lambda_w}(\omega^2 - \omega_{cz}^2)\right]f_i$$

$$-i\alpha_1 \sum_j A_{ij} f_j + \alpha_2 \sum_j S_{ij} f_j \ ,$$ (40)

where

$$A_{ij} = \int dz \frac{d\phi_i}{dz}\phi_j$$ (41)

and

$$S_{ij} = \int dz \, \phi_i \frac{d \ln\psi_0}{dz}\phi_j \ .$$ (42)

A_{ij} is an antisymmetric matrix ($A^T = -A$), while S_{ij} is symmetric ($S^T = S$). As a result, the right-hand side of Eq. (40) defines a Hermitian matrix:

$$H_{ij} = \frac{1}{2}\left[\omega^2 q^2 - (\vec{\omega}_c \cdot \mathbf{q})^2 + \frac{2\mu_i}{\lambda_w}(\omega^2 - \omega_{cz}^2)\right]\delta_{ij}$$

$$-i\alpha_1 A_{ij} + \alpha_2 S_{ij} \ .$$ (43)

We also note that $\tilde{M}_{ij}$ is a real symmetric matrix, as is its inverse, $\tilde{M}_{ij}^{-1}$.

We now establish that Eq. (40) admits solutions with real eigenmode frequencies. To prove this important result, we first consider the generalized eigenvalue problem

$$H\vec{v} = \lambda \tilde{M}^{-1}\vec{v} \ .$$ (44)

The matrix H and the eigenvalue λ are implicitly functions of the frequency, which we take to be a real parameter. If $\vec{v}^{(m)}$ and $\vec{v}^{(n)}$ are eigenvectors of Eq. (44) with eigenvalues λ_m and λ_n, respectively, then we can readily show using the Hermitian property of H and $\tilde{M}^{-1}$ that

$$(\lambda_n^* - \lambda_m) \sum_{ij} v_i^{(n)*} \tilde{M}_{ij}^{-1} v_j^{(m)} = 0 \ .$$ (45)

Setting $n = m$ in this equation, we see that the eigenvalue λ_m is real if the sum $\sum_{ij} v_i^{(m)*} \tilde{M}_{ij}^{-1} v_j^{(m)}$ is nonzero.

We next establish an important property of the matrix $\tilde{M}$. This matrix is in fact closely related to the energy functional in Eq. (1). Let us consider a trial density $n(\mathbf{r}) = n_0(\mathbf{r}) + \delta n(\mathbf{r})$, where $n_0(\mathbf{r})$ is the equilibrium solution of Eq. (4). Substituting this trial density into Eq. (1) and expanding in $\delta n(\mathbf{r})$ leads to

$$E[n] = E[n_0] + \int d\mathbf{r} \, \mu \delta n(\mathbf{r}) + \frac{1}{2}\int d\mathbf{r}\int d\mathbf{r}' \frac{\delta^2 E}{\delta n(\mathbf{r})\delta n(\mathbf{r}')}\bigg|_{n_0} \delta n(\mathbf{r})\delta n(\mathbf{r}') + \cdots \ .$$ (46)

The term linear in $\delta n(\mathbf{r})$ vanishes for a number-conserving fluctuation. Expanding the density fluctuation as

$$\delta n(\mathbf{r}) = 2 \sum_{\mathbf{q}} \sum_{i} c_i(\mathbf{q}) e^{i\mathbf{q}\cdot\mathbf{p}} \psi_0(z) \phi_i(z) \tag{47}$$

and substituting the result into Eq. (46), we find

$$E[n] = E[n_0] + A \sum_{\mathbf{q}} \sum_{ij} c_i^*(\mathbf{q}) \tilde{M}_{ij}(q) c_j(\mathbf{q}) + \cdots , \tag{48}$$

where $\tilde{M}$ is the matrix defined in Eq. (31), and A is the area of the slab. In this context, it is apparent that $\tilde{M}$ is just the inverse of the static density response function of the electronic system. Since $E[n]$ achieves an absolute minimum at $n = n_0$, the sum in Eq. (48) must be positive for an arbitrary fluctuation. Thus the matrix $\tilde{M}$ is positive definite and has positive eigenvalues only. This proves that the sum in Eq. (45) with $n = m$ is nonzero, and that the eigenvalues λ_m are indeed real. Finally, for distinct eigenvalues, the eigenvectors of Eq. (44) satisfy the orthogonality relation

$$\sum_{ij} v_i^{(n)*} \tilde{M}_{ij}^{-1} v_j^{(m)} = 0 . \tag{49}$$

Returning to Eq. (40), we expand $\vec{f}$ as $\sum_n a_n \vec{v}^{(n)}$ and make use of the orthogonality relation Eq. (49). We then find that the mode eigenfrequencies satisfy the equation

$$\omega^2(\omega^2 - \omega_c^2) = \lambda_n(\omega) . \tag{50}$$

The real solutions of Eq. (50), corresponding to real values of $\lambda_n(\omega)$, are the admissible mode frequencies.

We now establish the dependence of the mode frequencies on the direction of the magnetic field relative to the propagation wave vector. Since the states ϕ_i of the parabolic well have well-defined parity, the matrix $\tilde{M}$ has finite elements between states with the same parity, while the matrices S and A have finite elements between states of opposite parity. Grouping the states according to their parity, Eq. (44) can be displayed with the block structure

$$\begin{bmatrix} D_1 & \alpha_2 S - i\alpha_1 A \\ \alpha_2 S + i\alpha_1 A & D_2 \end{bmatrix} \begin{bmatrix} \vec{v}_1 \\ \vec{v}_2 \end{bmatrix}$$
$$= \lambda \begin{bmatrix} \tilde{M}_1^{-1} & 0 \\ 0 & \tilde{M}_2^{-1} \end{bmatrix} \begin{bmatrix} \vec{v}_1 \\ \vec{v}_2 \end{bmatrix} , \tag{51}$$

where $\vec{v}_1$ denotes the even-parity components and $\vec{v}_2$ the odd-parity components. The diagonal matrices D_1 and D_2 are invariant under the reversal of any magnetic-field component (note that $\mathbf{q} = q\hat{x}$), whereas either $\alpha_1 = \omega_{cx}\omega_{cz}q$ or $\alpha_2 = -\omega\omega_{cy}q$ will change sign. Taking the complex conjugate of Eq. (51) is equivalent to the replacement $\omega_{cx} \to -\omega_{cx}$ or $\omega_{cz} \to -\omega_{cz}$ in the matrix on the right-hand side of Eq. (51). Since λ is real, we see that the modes for these reversed field components have the same frequency as for the original field orientation, but the corresponding eigenvectors are complex conjugated. On the other hand, Eq. (51) can also be displayed as

$$\begin{bmatrix} D_1 & -\alpha_2 S - i\alpha_1 A \\ -\alpha_2 S + i\alpha_1 A & D_2 \end{bmatrix} \begin{bmatrix} \vec{v}_1^* \\ -\vec{v}_2^* \end{bmatrix}$$
$$= \lambda \begin{bmatrix} \tilde{M}_1^{-1} & 0 \\ 0 & \tilde{M}_2^{-1} \end{bmatrix} \begin{bmatrix} \vec{v}_1^* \\ -\vec{v}_2^* \end{bmatrix} . \tag{52}$$

Thus the eigenvalue at $-\omega_{cy}$ is the same as at ω_{cy}, while the two eigenvectors are related by the operation shown in Eq. (52). These conclusions depend crucially on the assumed symmetry of the equilibrium state. If the system is *not* invariant with respect to a reflection in the x-y plane, the modes will *not* possess the symmetries with respect to the direction of the magnetic field derived here.

Having established these general properties, we now consider various special cases of the magnetic-field and wave-vector dependences.

A. B=0, q=0

In this case we have $\alpha = 0$, and Eq. (37) reduces to

$$\lambda_w \omega^2 c_i = \sum_j \mu_i \tilde{M}_{ij} c_j , \tag{53}$$

with $\tilde{M}_{ij} = \tilde{M}_{ij}(0)$. Since $\mu_0 \equiv 0$, we see that the eigenvector with $c_0 \neq 0$ is associated with the mode $\omega = 0$. All other modes with nonzero frequencies have a vanishing ground-state wave-function amplitude. The significance of the $\omega = 0$ mode is revealed when we do the finite-q analysis which shows that it corresponds to the $q = 0$ 2D plasmon. The remaining modes in the $q = 0$ limit can be obtained by deleting the first row and first column of the matrix in Eq. (53), and considering only the coupling between terms with $i \neq 0$. The $q \to 0$ limit of Eq. (34) can then be taken with the result $(i, j \neq 0)$

$$M_{ij}^H(q \to 0) = -4\pi \int dz \int dz' \varphi_i(z) \psi_0(z) |z - z'|$$
$$\times \varphi_j(z') \psi_0(z') . \tag{54}$$

This integral is most easily evaluated by solving Poisson's equation to obtain the electric potential for the charge density $2\psi_0(z)\varphi_j(z)$ and then calculating the interaction with the charge density $\psi_0(z)\varphi_i(z)$. The remaining contributions M_{ij}^K and M_{ij}^X are readily obtained by quadrature and the eigenvalue problem is then solved using standard techniques.[37] We note that the structure of the coefficient matrix in Eq. (53) is $D(M + D)$, where D is the diagonal matrix of energy eigenvalues, μ_i. This matrix is not symmetric; however, applying the transformation $D^{-1/2}$ to the vector $\vec{c}$ leads to a coefficient matrix $D^{1/2} M D^{1/2} + D^2$ which is symmetric and positive definite. As a result, its eigenvalues are positive and the mode eigenfrequencies are necessarily real.

Since the modes of the parabolic well for $\mathbf{B} = 0$ have a well-defined parity, we can restrict the expansion of u to either even- or odd-parity states. The lowest odd-parity mode corresponds to the rigid oscillation of the equilibrium charge density about the center of the well. This can be demonstrated by returning to Eq. (24) with $\mathbf{q} = 0$ and $\omega_c = 0$, namely,

$$m^* \frac{\partial^2 \delta n}{\partial t^2} = -\frac{\partial}{\partial z}(n_0 \delta F_z) \ , \tag{55}$$

where δF_z is the change in the force acting on the fluid as a result of the density fluctuation. For a rigid displacement of the charge density, $n(z,t) = n_0[z - \eta(t)]$ and $\delta n(z,t) = -n_0'(z)\eta(t)$. Also,

$$\delta F_z(z,t) = F_z(n_0[z - \eta(t)]) = F_z^{\mathrm{int}}(n_0[z - \eta(t)]) - kz$$
$$= -k\eta(t) \ ,$$

where we have used the fact that $F_z^{\mathrm{int}}[n_0(z)] - kz = 0$ in equilibrium. Here, F_z^{int} is the internal force exclusive of the force arising from the external confining potential. Equation (55) thus reduces to

$$m^* \frac{d^2 \eta}{dt^2} = -k\eta \ , \tag{56}$$

which shows that the mode has the frequency $\omega_0 = \sqrt{k/m^*}$ of the bare harmonic potential. This rigid oscillation of the center of mass is a general feature of parabolic confinement and shows that the generalized Kohn's theorem[29] is satisfied by the TFDW hydrodynamics. It is important to realize, however, that this result only follows if the dynamics is consistent with the true equilibrium charge density of the system. Choosing an arbitrary density profile $n_0(z)$ will not generate the correct dynamical behavior regardless of how "reasonable" the density appears to be. On the other hand, the results need not be unphysical since one can always view the chosen $n_0(z)$ as corresponding to some different external potential. Thus in more complicated situations, the strategy of calculating the dynamics for a guessed equilibrium density might well be useful.

The above result for the center-of-mass mode can also be demonstrated directly using Eq. (53). By truncating the expansion of u at ν terms, Eq. (53) generates ν distinct eigenvalues. The accuracy of the eigenvalues and the corresponding eigenvectors will increase with increasing ν. For example, we find that the center-of-mass mode frequency rapidly converges to the correct value ω_0. We can also demonstrate this convergence by plotting the amplitude of the center-of-mass mode for the sequence $\nu = 3$, 5, and 7 in Fig. 5; on the scale of Fig. 5, the amplitude with 11 terms in the expansion is virtually indistinguishable from $n_0'(z)$. Since the amplitude of the density fluctuation is localized near the edges of the slab, more terms are required in the expansion as the width of the slab increases. In the MTF limit, the equilibrium density is constant between $z = -W/2$ and $W/2$, and zero otherwise. The corresponding center-of-mass density fluctuation therefore consists of δ functions at the edges of the slab. Our result in TFDW is qualitatively similar, but the δ functions are broadened into a smooth and continuous distribution. This behavior is of course physically more realistic, and demonstrates that TFDW is a useful approximation to the true quantum-mechanical response.

In Fig. 6 we illustrate a few of the higher modes which are all converged with respect to the number of basis functions. These modes are again qualitatively similar to the results of DH in the MTF limit. They consist of sur-
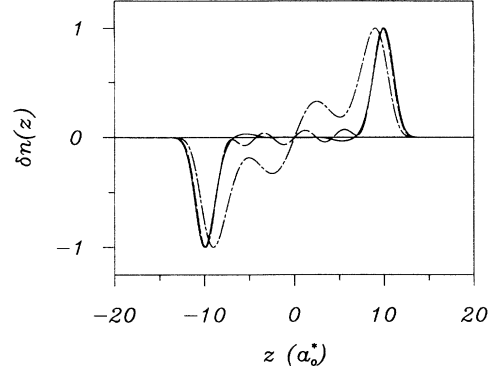
FIG. 5. Illustration of the convergence of the center-of-mass mode density at $q = 0$, with the number of basis functions used in the expansion. The dash-dotted line is for $\nu = 3$, the dashed line is for $\nu = 5$, and the solid line is for $\nu = 7$. In this and subsequent figures, the well parameters are those of Fig. 3.

face charge fluctuations together with charge fluctuations in the interior of the slab corresponding to bulk-plasmon standing waves. Due to the numerical nature of the equilibrium calculations, we cannot give analytic expressions for the mode frequencies, ω_n.

B. $B \neq 0$, $q = 0$

In this case, Eq. (37) reduces to the simple form

$$\lambda_w \frac{\omega^2(\omega^2 - \omega_c^2)}{\omega^2 - \omega_{cz}^2} c_i = \sum_j \mu_i \widetilde{M}_{ij} c_j \ . \tag{57}$$

Since the $\widetilde{M}_{ij}$ matrix does not mix states with different parity, the modes again have well-defined even or odd parity. Furthermore, all the effects of the magnetic field
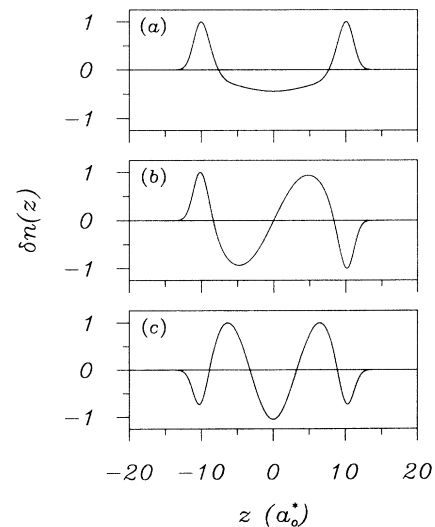
FIG. 6. Normalized density fluctuations for higher-lying modes at $q = 0$. (a) The first excited even-parity mode, (b) first excited odd-parity mode, and (c) second excited even-parity mode.

are included in the frequency-dependent factor on the left-hand side of Eq. (57). Since Eq. (57) has the same form as Eq. (53), this factor is equal to one of the eigenvalues ω_n^2 of the zero-field case. As a result, the mode frequencies at finite field are given by

$$\omega_{n\pm}^2(B)=\tfrac{1}{2}(\omega_c^2+\omega_n^2)\pm\tfrac{1}{2}\sqrt{(\omega_c^2+\omega_n^2)^2-4\omega_{cz}^2\omega_n^2}\ . \tag{58}$$

This expression has exactly the same form as found previously in the MTF approximation and differs only in the values of the zero-field eigenvalues ω_n^2 which appear. Later in Figs. 9 and 10 we show the q dependence of the modes for various magnetic fields. The limiting frequencies for $q\rightarrow0$ are given in all cases by Eq. (58), as shown in Fig. 10(g).

Each of the two $\omega_{n\pm}(B)$ modes has the same eigenvector and therefore the same density fluctuation. However the two modes are distinguished by the associated velocity field. From Eqs. (17) and (20), we find the ratios

$$\frac{v_y}{v_x}=\frac{i\omega}{\omega_{cz}} \tag{59}$$

and

$$\frac{v_z}{v_x}=\frac{\omega_{cz}^2-\omega^2}{\omega_{cx}\omega_{cz}}\ . \tag{60}$$

Here we assume that **B** lies in the x-z plane and makes an angle θ with respect to the z axis. Substituting the mode frequencies $\omega_{n\pm}$ into these expressions determines the relative amplitudes of the velocity components. For example, for $\theta\rightarrow0$, v_z/v_x tends to zero for both the $n+$ modes with $\omega_n<\omega_c$, and for the $n-$ modes with $\omega_n>\omega_c$. This set of modes has the limiting frequency ω_c and therefore corresponds to cyclotron motion in the x-y plane. The z dependence of the velocity components in this limit is arbitrary. The remaining modes have the limiting frequencies ω_n as $\theta\rightarrow0$, and only have a finite z component of the velocity field. These modes are just the normal oscillations considered in Sec. III A, and are not affected by the magnetic field since the motion of the electrons occurs along the field direction.

In the opposite limit of $\theta\rightarrow\pi/2$, the $n-$ mode frequencies tend to zero while the $n+$ mode frequencies tend to $\sqrt{\omega_c^2+\omega_n^2}$. For the $n-$ modes only the x component of the velocity field is finite; that is, along the field direction in the plane of the slab. The mode frequencies are zero since there is no restoring force in the x direction, and the motion is a pure translation. The $n+$ modes, on the other hand, correspond to motion in the y-z plane and are bulk magnetoplasmon standing waves. Interestingly, these waves have the same z-dependent density fluctuations as in the **B**$\rightarrow0$ limit, in spite of the fact that the magnetic field gives rise to a cyclotron type of motion. These results are analogous to those found in the MTF limit.

C. B=0, q≠0

In this case, Eq. (37) reduces to the form

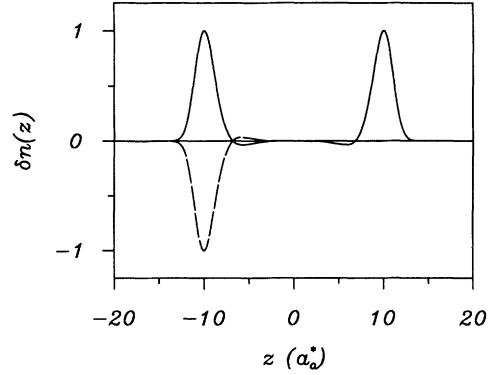$$\lambda_w\omega^2c_i=\sum_j\mu_i(q)\tilde{M}_{ij}(q)c_j\ , \tag{61}$$

FIG. 7. Comparison of the **q**=0 density fluctuations of the 2D plasmon (solid) and center-of-mass mode (dash). The two mode densities cannot be distinguished on the right-hand side of the figure.

where $\mu_i(q)=\mu_i+\tfrac{1}{2}\lambda_wq^2$. This equation is also of the same form as Eq. (53), and the same procedure is used to obtain the mode frequencies. To see the behavior in the $q\rightarrow0$ limit, we note that

$$\mu_0(q)M_{00}(q)=2\pi\lambda_wn_{2D}q+O(q^2), \tag{62}$$

while $\mu_0(q)M_{0j}(q)$ is of order q^2. As a result, the $i=0$ equation in Eq. (61) reduces, to lowest order in q, to

$$\lambda_w\omega^2c_0=2\pi\lambda_wn_{2D}qc_0+O(q^2)\ , \tag{63}$$

which shows that the frequency of the lowest mode is just the 2D plasmon

$$\omega_{2D}^2=2\pi n_{2D}q\ . \tag{64}$$

Restoring the physical parameters, $\omega_{2D}^2=2\pi e^2n_{2D}q/m^*\epsilon$.

Even though the frequency as given by Eq. (63) in the long-wavelength limit is independent of the coefficients with $i\neq0$, the density fluctuation is still an admixture of
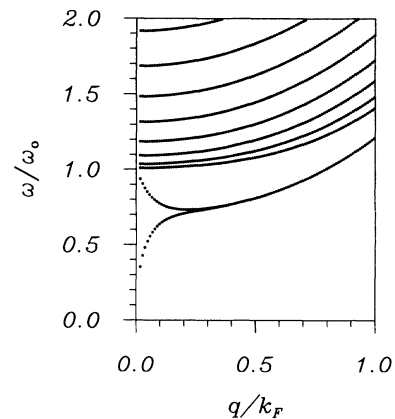

FIG. 8. The dispersion of the mode frequencies with wave vector q at $B=0$. The lowest mode is the 2D plasmon which merges with the center-of-mass mode at higher wave vectors as these two modes evolve, respectively, into the symmetric and antisymmetric surface plasmons of the slab.

several even-parity states. To determine the mode eigenvector in the $q \to 0$ limit, we set $\omega = 0$ and solve Eq. (61) with c_0 assigned an arbitrary value. The resulting density fluctuation is plotted in Fig. 7 together with the density fluctuation for the $n = 1$ mode. The figure shows that the $n = 0$ density fluctuation is proportional to $n'_0(z)$ at each edge of the slab. In other words, the $n = 0$ mode constitutes a local expansion or contraction of the slab width which is periodically modulated in the direction of the propagation wave vector, corresponding to the flow of electrons parallel to the plane of the slab.

Figure 8 shows the dispersion of the modes up to a maximum value of the wave vector equal to the 3D Fermi wave vector. The 2D plasmon has a $q^{1/2}$ dispersion and at higher wave vectors, merges with the $n = 1$ center-of-mass mode. By this point, the $n = 0$ and 1 modes have become the symmetric and antisymmetric surface-plasmon modes of the slab and are degenerate since the density fluctuations on opposite sides of the slab are essentially uncoupled. Unlike the MTF limit in which the modes asymptotically approach $\omega_{3D}/\sqrt{2}$, the surface-plasmon modes have a positive q dispersion for which the von Weizsäcker correction is mainly responsible. However, the form of Eq. (61) does not permit a sim-
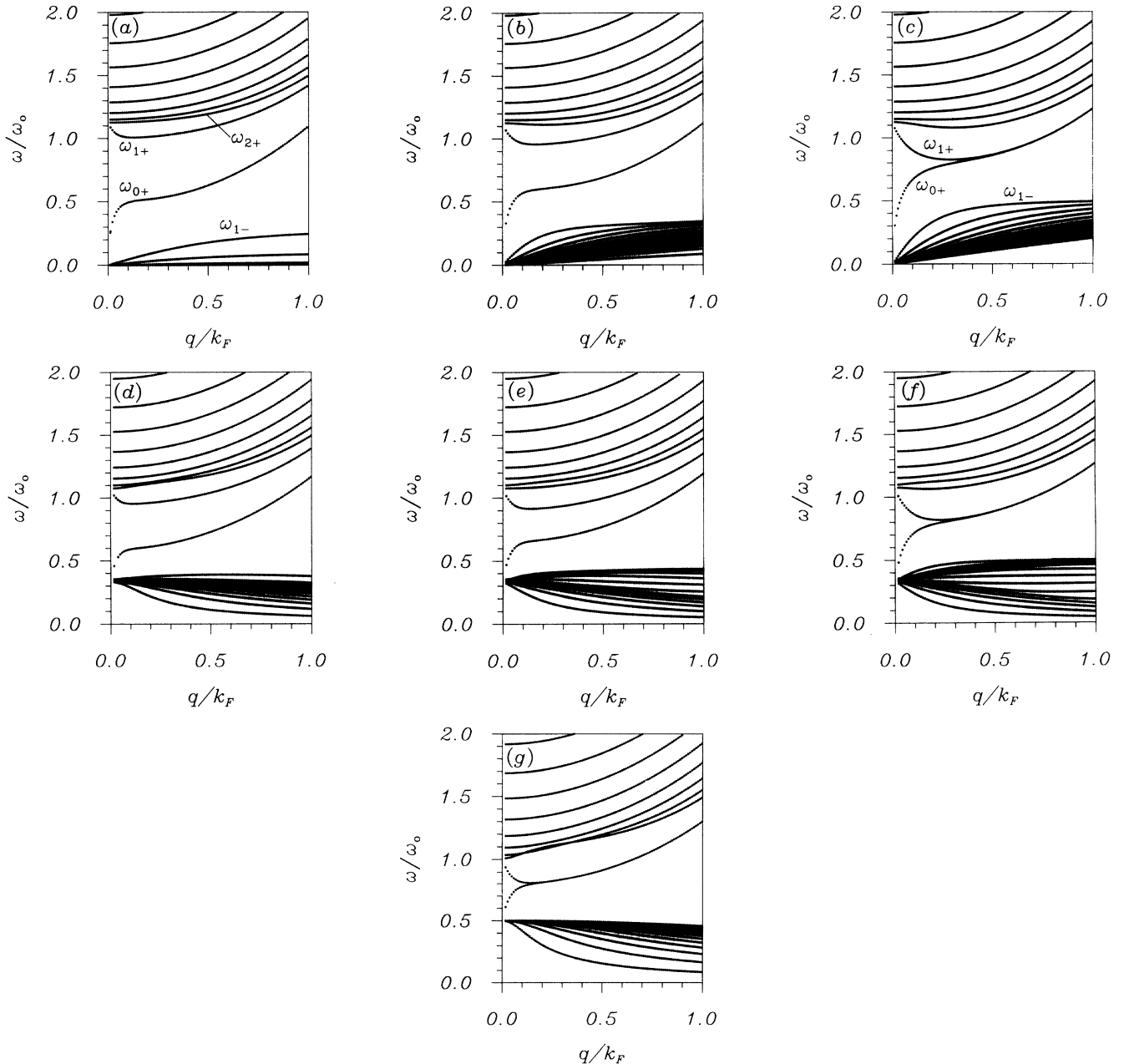

FIG. 9. Wave-vector dependence of the magnetoplasmon modes for $\omega_c/\omega_0 = 0.5$ for various orientations of the magnetic field. (a) $\theta = 90°$, $\phi = 90°$; (b) $\theta = 90°$, $\phi = 45°$; (c) $\theta = 90°$, $\phi = 0°$; (d) $\theta = 45°$, $\phi = 90°$; (e) $\theta = 45°$, $\phi = 45°$; (f) $\theta = 45°$, $\phi = 0°$; and (g) $\theta = 0°$.

ple attribution of the wave-vector dispersion to one particular source, and in the case of the higher modes, both the TF pressure and the von Weizsäcker correction are having an important effect.

D. $B \neq 0, q \neq 0$

Finally we return to the general dependence of the modes on q and B as determined by the solution of Eq. (37). Qualitatively, our results are very similar to those obtained by DH,[28] who give a thorough discussion of the magnetoplasmon excitations in parabolic wells. Here we will elaborate only on some of the features which differ from their results. In Figs. 9(a)–9(g) and 10(a)–10(g) we

show the mode dispersions for a sampling of magnetic-field directions and magnitudes. The parameters used in these figures were chosen to correspond closely to those of DH in order to facilitate a direct comparison.

One of the main differences between the two sets of calculations concerns the dispersion of the $n = 0$ and 1 surface modes, which are generally distinguished in Figs. 9 and 10 by their separation from the bulk bands. For $\omega_c < \omega_0$, the surface modes appear between the upper and lower bulk bands which emanate from the frequencies defined by Eq. (58), while for $\omega_c > \omega_0$ there is a more complicated overlap and mixing of the surface and bulk modes. In the MTF approximation, the surface modes are somewhat easier to identify since their frequencies ap-
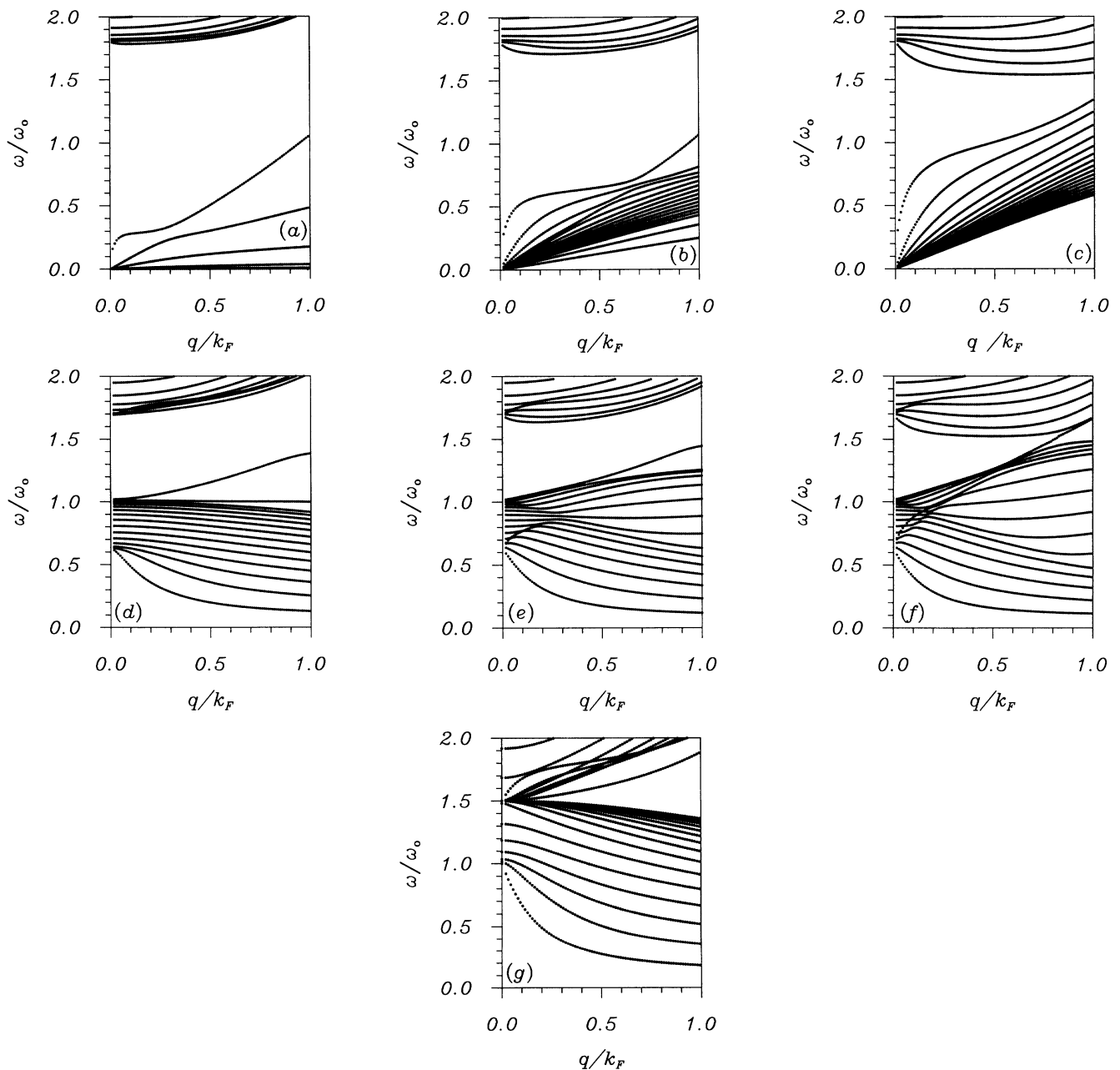

FIG. 10. As in Fig. 9, but for $\omega_c/\omega_0 = 1.5$.

proach a constant value for large wave vectors. In TFDW, however, the modes exhibit a positive dispersion and approach the bulk modes at large wave vectors, as previously seen in the $B=0$ case. An unambiguous identification of the modes of course requires an examination of the mode density fluctuations which we will display for a few cases.

As seen in Figs. 9(c), 9(f), and 9(g), the two surface modes merge at large wave vectors when there is no in-plane component of the magnetic field which is perpendicular to the wave vector q. For these orientations the quantity α_2 defined in Eq. (25) is zero. As soon as α_2 acquires a finite value as in Figs. 9(a), 9(b), 9(d), and 9(e), the two surface modes remain separated at large wave vectors. In Fig. 11 we examine the character of the two surface modes for the particular case of Fig. 9(a) at a few values of q. The density fluctuation for these modes is asymmetric with respect to the midpoint of the slab, as are all the modes when $\alpha \neq 0$. The lower surface mode is seen to be localized at the lower edge of the slab (see Fig. 4) for all values of the wave vector between $0.1k_F$ and k_F with a width that increases with increasing q. For small q, the upper surface mode takes on the character of the center-of-mass mode, as discussed in Sec. III B and shown in Fig. 11(a). However, for larger q, the density fluctuation is localized at the upper edge of the slab and becomes broader with increasing q.

At first sight these surface modes might seem unusual but they have a straightforward interpretation. A bounded three-dimensional electron gas in the presence of a magnetic field parallel to the surface supports two edge magnetoplasmons, as discussed for example by Fetter.[38] These modes are localized at the surface and have the peculiar property that for a given wave vector and magnetic-field orientation, the mode frequencies have op-

posite signs and correspond to waves traveling in opposite directions. These modes will of course also be present in a slab when the modes on opposite sides of the slab are decoupled, as they are when the slab is sufficiently thick or when the wave vector is sufficiently large. In our analysis, we extract only the positive roots representing waves traveling in the direction of q. For the geometry being considered, the ω_{1+} mode in Fig. 9(a) has a positive frequency and is the mode localized on the upper edge as displayed in Fig. 11. The other surface mode localized at this surface has a negative frequency, but on the opposite side of the slab the direction of the magnetic field is reversed relative to the plane defined by q and the surface normal, and for this configuration the lower mode has a positive frequency (ω_{0+}). Thus for a given q and B, the two modes which propagate in the same direction are localized on opposite sides of the slab. This identification is also consistent with the fact that the decay length of the density fluctuation is smaller for the low-frequency mode than it is for the high-frequency mode,[38] as is clearly evident in Fig. 11.

Another feature of interest in Fig. 9(a) is the dispersion of the lower band of bulk modes which, in the MTF approximation, are all undispersed with zero frequency. The additional dispersion observed here is a consequence of the diffuseness of the surface electron density which in turn is due to the von Weizsäcker correction to the kinetic energy. In fact, a plot of the density fluctuation in Fig. 12 reveals that the uppermost mode in the lower bulk band is also a surface mode. The small-scale oscillations seen in these figures are not real, as was checked by repeating the calculation for several dimensions of the matrix problem, and are due to the finite number of basis functions used in the calculation. At small wave vectors, this mode has the character of what can be called a surface dipole mode as opposed to the surface monopole discussed above. At larger wave vectors, the dipole character of this mode diminishes and it looks more like the
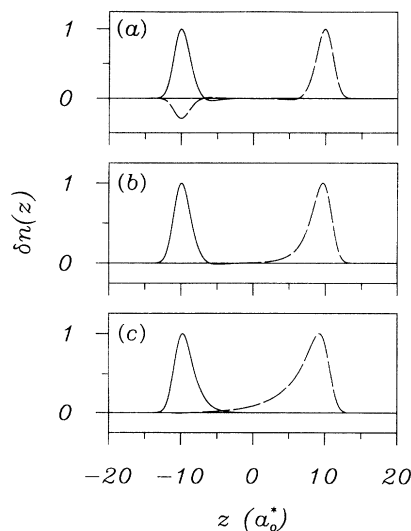

FIG. 11. Mode-density fluctuations for the surface magnetoplasmons corresponding to the conditions in Fig. 9(a). The solid line is the low-frequency mode labeled ω_{0+} in Fig. 9(a), and the dashed lined is the ω_{1+} mode. The values of the wave vectors are (a) $q=0.1k_F$, (b) $q=0.5k_F$, and (c) $q=k_F$.
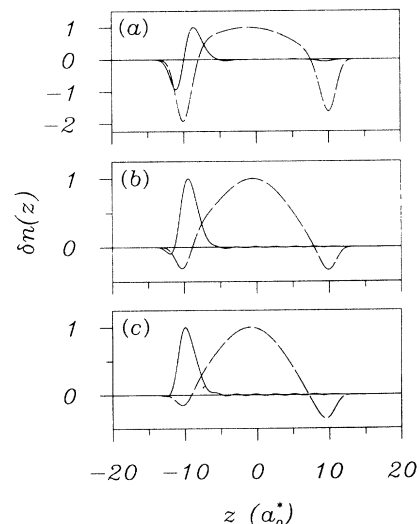

FIG. 12. As in Fig. 11, but for the ω_{1-} (solid) and ω_{2+} (dashed) modes.

lower surface mode in Fig. 11. Despite the similarity of the density fluctuations for these two modes, they have different frequencies and therefore distinct velocity distributions. The appearance of an additional surface mode can be likened to the onset of a bound state in a quantum-mechanical scattering calculation in which the strength of an attractive scattering potential is systematically increased. In the present context, the diffuseness of the surface has made it possible for a continuum bulk mode to be localized at the surface. All other modes displayed in Fig. 9(a) are bulk modes which have a significant density fluctuation throughout the slab. An example of such a mode is also shown in Fig. 12.

The dispersion curves shown in Figs. 9(b) and 9(c) are very similar to those presented by DH. One difference is that the lower band of bulk modes has an accumulation line which is displaced away from the q axis. Although we have not been able to establish this analytically, we find that the lowest mode tends to a finite frequency at finite q as the dimension of the eigenmode problem is increased. For the geometry of Fig. 9(c), $\alpha = 0$ and, as a consequence, the modes have well-defined parity. In Fig. 13 we show the two surface modes in this geometry and the highest frequency bulk mode in the lower band. We see that the character of the latter has changed significantly with the rotation of the magnetic field in the plane of the slab from a direction perpendicular to **q**, to one that is parallel, by which point it is clearly a bulk mode [cf. Fig. 12(a)].

Starting with **B**∥**q** and tilting the magnetic field out of the plane toward the surface normal, the dispersion of the modes varies progressively as shown in Figs. 9(c), 9(f), 9(g), 10(c), 10(f), and 10(g). At either end of this range, $\alpha = 0$ and the density fluctuations have a well-defined parity. However, at intermediate orientations of the magnetic field, as in Figs. 9(f) and 10(f), $\alpha_2 = 0$ but $\alpha_1 \neq 0$ and the modes do not have a definite parity. In fact, as can b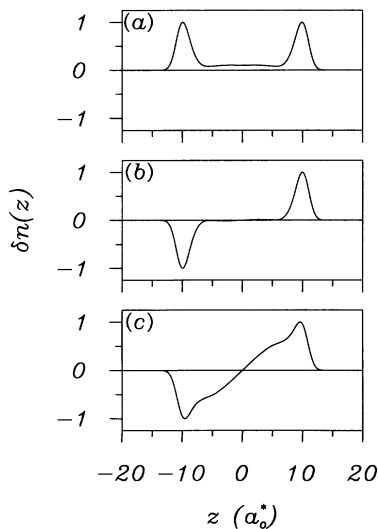e seen from the structure of Eq. (51), the density fluctuation for these orientations is complex valued, with the two parity components being 90° out of phase.

For $\omega_c < \omega_0$, two surface modes lie in the gap between the lower and upper bulk bands, as shown in Figs. 9(c), 9(f), and 9(g). At small q, the lower surface mode is the 2D magnetoplasmon, and the upper mode is still essentially the center-of-mass mode. As q increases, these two modes merge as the density fluctuations on either side of the slab become uncoupled and the modes take on the character of surface magnetoplasmons for a three-dimensional half-space. In the Faraday geometry of Fig. 9(g), the 2D magnetoplasmon starts from ω_c at $q = 0$, while the center-of-mass mode starts at ω_0. Figures 10(c), 10(f), and 10(g) show that the situation for $\omega_c > \omega_0$ is more complex. For the simpler Faraday geometry, the cyclotron frequency lies in the midst of the bulk-plasmon frequencies, and a gap between the upper and lower bulk bands does not persist to $q = 0$. As a result, the surface modes are strongly mixed with the bulk modes. This is particularly evident in Fig. 10(f), where the lower surface mode appears to be running through the lower bulk band near $q = 0$. This line is a sequence of sharp anticrossings which are not resolved for the mesh of q points used in this figure, and is actually very similar to the second set of anticrossings clearly visible at larger wave vectors. The double set of anticrossings in Fig. 10(f) differs from the MTF approximation, in which only a single set of anticrossings is observed.

As a final point, we emphasize that all modes obtained in Figs. 9 and 10 were obtained using a finite basis in the solution of Eq. (37), and that additional modes appear as more terms in the expansion are retained. This truncation may lead to apparent differences between the modes obtained here and by DH. For example, in Fig. 10(g), the use of a larger basis set will lead to an accumulation line at the cyclotron frequency, parallel to the q axis, and not to the downward sloping line seen in the figure. However, the important differences between the two sets of calculations which we have identified so far are independent of the number of terms used in the basis set expansion. Most of the differences can be traced to the diffuseness of the equilibrium surface density which arises beyond the MTF approximation; that is, for the fully nonlinear TFDW theory.

IV. POWER ABSORPTION

Having discussed the modes which occur under various conditions, we now address the question of what is observed in an experimental measurement.[39–43] We study the situation in which radiation is incident normally on the confining well. In this configuration, the quantity measured is usually the transmitted intensity which is a direct measure of the power absorbed by the electron gas. The instantaneous power absorption is given by

$$P(t) = \int d\mathbf{r}\, \mathbf{j}(\mathbf{r},t) \cdot \mathbf{E}^{\text{ext}}(t) \ , \qquad (65)$$

where $\mathbf{j}(\mathbf{r},t)$ is the current induced by the external electromagnetic field which we take to be spatially uniform over the extent of the sample and polarized in the x direction: $\mathbf{E}^{\text{ext}}(t) = \frac{1}{2}E_0(e^{-i\omega t} + e^{i\omega t})\hat{\mathbf{x}}$. Making use of the fact

FIG. 13. Mode-density fluctuations corresponding to the conditions in Fig. 9(c) at the wave vector $q = 0.1 k_F$. (a) ω_{0+} mode, (b) ω_{1+} mode, and (c) ω_{1-} mode.

that the induced current only depends on the z coordinate, the time-averaged power absorption per unit area is

$$\frac{\bar{P}}{A} = \tfrac{1}{2}E_0 \, \mathrm{Re} \int dz \, j_x(z) \, . \tag{66}$$

Using $j_x(z) = -en_0(z)v_x(z)$, the power absorption can be expressed in terms of the velocity field, which we now assume is governed by the equation

$$m^* n_0 \frac{\partial \mathbf{v}}{\partial t} = -m^* n_0 \gamma \mathbf{v} + n_0 \delta \mathbf{F} - en_0 \frac{\mathbf{v}}{c} \times \mathbf{B} \, . \tag{67}$$

Here γ is a phenomenological relaxation rate which accounts for both momentum nonconserving scattering processes and internal energy relaxation associated with single-particle excitations. In addition to the force defined in Eq. (16), $\delta \mathbf{F}$ also contains a term, $-e\mathbf{E}^{\mathrm{ext}}$ which accounts for the coupling of the electron gas to the external field. Because of the relaxation rate, the frequency ω appearing in Eq. (17) is now replaced by $\tilde{\omega} = \omega + i\gamma$. Using Eq. (17) and the $q = 0$ limit of Eqs. (19) and (20), the power absorption can finally be expressed as

$$\frac{\bar{P}}{A} = -\tfrac{1}{2}eE_0 \, \mathrm{Re} \left[\frac{\omega(\tilde{\omega}\omega_{cy} + i\omega_{cx}\omega_{cz})}{\tilde{\omega}^2 - \omega_{cz}^2} \int dz \, z \delta n(z) \right.$$
$$\left. - \frac{n_{2D}eE_0}{2m^*} \frac{i\tilde{\omega}}{\tilde{\omega}^2 - \omega_{cz}^2} \right] \, . \tag{68}$$

This result shows that the interesting part of the power absorption is given by the induced dipole moment of the electron slab.

In the Voigt geometry $\mathbf{B} = B\hat{\mathbf{y}}$, Eq. (68) reduces to

$$\frac{\bar{P}}{A} = -\tfrac{1}{2}eE_0 \, \mathrm{Re} \left[\frac{\omega\omega_c}{\tilde{\omega}} \int dz \, z\delta n(z) \right]$$
$$+ \frac{n_{2D}e^2E_0^2}{4m^*} \frac{\gamma}{\omega^2 + \gamma^2} \, . \tag{69}$$

For $\omega_c \to 0$, the first term vanishes, leaving only the Drude absorption given by the second term. In the case of the Faraday geometry with $\mathbf{B} = B\hat{\mathbf{z}}$, Eq. (68) reduces to

$$\frac{\bar{P}}{A} = \frac{n_{2D}e^2E_0^2}{8m^*} \left[\frac{\gamma}{(\omega - \omega_c)^2 + \gamma^2} + \frac{\gamma}{(\omega + \omega_c)^2 + \gamma^2} \right] \, . \tag{70}$$

In this geometry, the external field does not induce a density fluctuation, and the absorption occurs only at the cyclotron resonance. Finally, we present the result for the somewhat artificial case in which the system is subjected to a uniform external field which is polarized in the z direction; that is, normally to the plane of the slab. We find

$$\frac{\bar{P}}{A} = \tfrac{1}{2}eE_0 \, \mathrm{Re} \left[i\omega \int dz \, z\delta n(z) \right] \, . \tag{71}$$

We now consider the evaluation of Eq. (68) for the general magnetic-field orientation. Because of the external driving field, the expansion coefficients of the induced density c_i no longer satisfy the homogeneous equation given in Eq. (57). Instead, we have the inhomogeneous equation

$$\sum_j \mu_i \tilde{M}_{ij} c_j - \lambda_w \frac{\omega\tilde{\omega}(\tilde{\omega}^2 - \omega_c^2)}{\tilde{\omega}^2 - \omega_{cz}^2} c_i$$
$$= -\lambda_w \frac{\tilde{\omega}\omega_{cy} - i\omega_{cx}\omega_{cz}}{\tilde{\omega}^2 - \omega_{cz}^2} p_{i0} \, , \tag{72}$$

where

$$p_{i0} = \int dz \, \phi_i \frac{d\phi_0}{dz} \, . \tag{73}$$

We have here scaled the inhomogeneous term to allow the power absorption to be written in the convenient form

$$\frac{\bar{P}}{A} = \frac{n_{2D}e^2E_0^2}{2m^*} \, \mathrm{Im} \left[\frac{\omega(\tilde{\omega}\omega_{cy} + i\omega_{cx}\omega_{cz})}{\tilde{\omega}^2 - \omega_{cz}^2} \sum_i d_{i0}c_i \right.$$
$$\left. - \frac{\tilde{\omega}}{2(\tilde{\omega}^2 - \omega_{cz}^2)} \right] \, , \tag{74}$$

with

$$d_{i0} = \int dz \, \phi_i z\phi_0 \, . \tag{75}$$

d_{i0} is the dipole matrix element coupling the ground state to higher excited states.

Since we have made no assumption regarding the shape of the confining potential, the result in Eq. (74) is in fact quite general. To solve Eq. (72), we introduce the orthonormal eigenvectors defined by

$$(D^{1/2}MD^{1/2} + D^2)\vec{w}^{(n)} = \lambda_w \omega_n^2 \vec{w}^{(n)} \, , \tag{76}$$

where D is again the diagonal energy matrix ($D_{ij} = \mu_i \delta_{ij}$). In terms of these eigenvectors, the solution vector of Eq. (72) is given by

$$\vec{c} = \sum_n a_n D^{1/2} \vec{w}^{(n)} \, , \tag{77}$$

where

$$a_n = \frac{\tilde{\omega}\omega_{cy} - i\omega_{cx}\omega_{cz}}{\omega\tilde{\omega}(\tilde{\omega}^2 - \omega_c^2) - \omega_n^2(\tilde{\omega}^2 - \omega_{cz}^2)} (\vec{w}^{(n)}, D^{-1/2}\vec{p}) \, . \tag{78}$$

The bracket denotes an inner product of two vectors, and the vector $\vec{p}$ has components p_{i0}. With this result, the sum in Eq. (74) can be expressed as

$$\sum_i d_{i0}c_i = \sum_n \frac{\tilde{\omega}\omega_{cy} - i\omega_{cx}\omega_{cz}}{\omega\tilde{\omega}(\tilde{\omega}^2 - \omega_c^2) - \omega_n^2(\tilde{\omega}^2 - \omega_{cz}^2)}$$
$$\times (\vec{w}^{(n)}, D^{1/2}\vec{d})(\vec{w}^{(n)}, D^{-1/2}\vec{p}) \, , \tag{79}$$

where the vector $\vec{d}$ has components d_{i0}.

Equation (79) simplifies in the case of a parabolic well since $d\phi_0/dz$ is the $n = 1$ mode amplitude and the inhomogeneous vector in Eq. (72) is proportional to $D^{1/2}\vec{w}^{(1)}$. As a result, Eq. (77) reduces to a single term and

$$c_i = \frac{\tilde{\omega}\omega_{cy} - i\omega_{cx}\omega_{cz}}{\omega\tilde{\omega}(\tilde{\omega}^2 - \omega_c^2) - \omega_1^2(\tilde{\omega}^2 - \omega_{cz}^2)} p_{i0} \, . \tag{80}$$

In other words, the induced density has a spatial amplitude precisely that of the $n = 1$ eigenmode, and is resonant at the cyclotron-shifted frequencies given by Eq. (58). Substituting Eq. (80) into the expression for the power absorption in Eq. (74), we obtain

$$\frac{\bar{P}}{A} = \frac{n_{2D}e^2 E_0^2}{2m^*} \text{Im} \left[\frac{\omega(\tilde{\omega}^2\omega_{cy}^2 + \omega_{cx}^2\omega_{cz}^2)}{(\tilde{\omega}^2 - \omega_{cz}^2)[\omega\tilde{\omega}(\tilde{\omega}^2 - \omega_c^2) - \omega_1^2(\tilde{\omega}^2 - \omega_{cz}^2)]} \sum_i d_{i0}p_{i0} - \frac{\tilde{\omega}}{2(\tilde{\omega}^2 - \omega_{cz}^2)} \right] . \tag{81}$$

To simplify Eq. (81) further, we note that

$$\sum_i d_{i0}p_{i0} = -\tfrac{1}{2} , \tag{82}$$

which, with the identification of d_{i0} and p_{i0} as dipole and momentum matrix elements, respectively, is essentially a statement of the Thomas-Reiche-Kuhn (or f) sum rule.[44] As a result, Eq. (81) finally yields

$$\frac{\bar{P}}{A} = \frac{n_{2D}e^2 E_0^2}{4m^*} \text{Im} \left[\frac{\omega(\tilde{\omega}^2 - \omega_{cx}^2) - \tilde{\omega}\omega_1^2}{\omega_1^2(\tilde{\omega}^2 - \omega_{cz}^2) - \omega\tilde{\omega}(\tilde{\omega}^2 - \omega_c^2)} \right] . \tag{83}$$

This expression demonstrates that $\bar{P}/A$ is resonant only at the center-of-mass mode frequencies, and not at $\tilde{\omega} = \pm\omega_{cz}$, as Eq. (81) would seem to suggest. The necessary cancellation of the singularities at $\tilde{\omega} = \pm\omega_{cz}$ depends critically on the validity of the f-sum rule. The same result can also be shown to hold for an arbitrary confining potential by considering the limit of Eq. (79) as $\tilde{\omega} \rightarrow \pm\omega_{cz}$.

The power absorption as given by Eq. (83) can be calculated easily for various orientations of the magnetic field. The positions of the absorption peaks depend only on the polar angle θ, but the intensity is also a strong function of the azimuthal angle ϕ and the magnitude of the ratio ω_c/ω_0. As the magnetic field is tilted away from the z axis in the x-z plane, the cyclotron peak splits into two peaks at the frequencies $\omega_\pm(B)$. If $\omega_c/\omega_0 < 1$, most of the oscillator strength remains with $\omega_-(B)$,
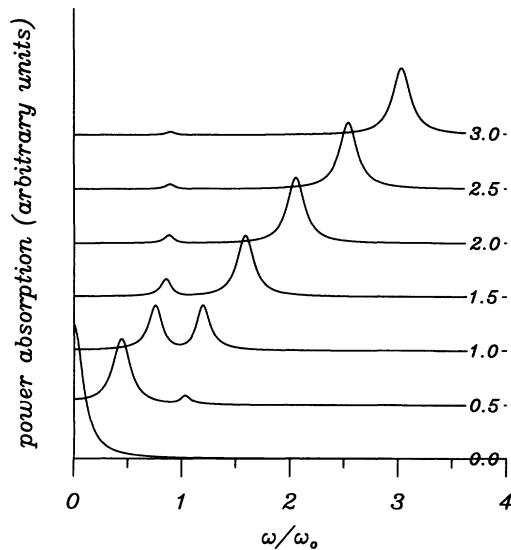
which shifts down from the cyclotron frequency with increasing θ and eventually turns into the Drude peak centered at zero frequency. On the other hand, if $\omega_c/\omega_0 > 1$, the $\omega_-(B)$ mode continually builds in intensity as the polar angle approaches 90°, at the expense of the $\omega_+(B)$ mode. The situation is somewhat different when the magnetic field is tilted in the y-z plane. The $\omega_+(B)$ mode persists with a finite intensity up to $\theta = 90°$. At this polar angle, the Drude peak also has a finite intensity, but its width is reduced by a factor $(1 + \omega_c^2/\omega_1^2)^{-1}$, and it therefore becomes less intense with increasing magnetic field. A subset of this behavior is illustrated in Fig. 14, which shows the power absorption for a fixed magnetic-field orientation, but for a range of magnetic-field strengths. At low-field strengths, the oscillator strength is concentrated in the ω_- mode, but shifts to the ω_+ mode as the field is increased until finally at high fields the absorption follows the cyclotron resonance.

V. CONCLUSIONS

In this paper we have demonstrated the possibility of developing a realistic hydrodynamic description of the collective excitations in inhomogeneous systems. Earlier attempts to achieve this objective have generally met with limited success because of their failure to properly account for the equilibrium properties of the system. In our work we have made use of the Thomas–Fermi–Dirac–von Weizsäcker approximation which is capable of providing realistic ground-state electronic densities. Deviations of the density from the ground-state distribution lead to internal forces which tend to drive the density back toward its equilibrium state. It is these forces, consistently determined from the ground-state distribution, which must be used in the hydrodynamic description. The use of an arbitrary density distribution which is incompatible with the assumed equation of state can lead to spurious internal forces and unphysical collective behavior. This failing has been encountered in earlier applications,[12,15] but is not an intrinsic limitation of the hydrodynamic approach.

We have applied the general hydrodynamic theory to determine the magnetoplasmon excitations of a parabolically confined electron gas. At long wavelengths $(q \rightarrow 0)$, we have demonstrated that the modes are consistent with the generalized Kohn theorem[29] which stipulates that the dipole-allowed excitation is simply the center-of-mass mode with frequency given by Eq. (58) for $n = 1$. This result is more general than the demonstration provided by Dempsey and Halperin,[28] which is based on the model of an electron slab with a discontinuous density profile. Furthermore, we have developed an efficient method for solving the hydrodynamic equations which makes use of

FIG. 14. Power absorption as a function of frequency. The curves are labeled by the ratio ω_c/ω_0 in the range 0–3. The orientation of the magnetic field is given by $\theta = 25°$ and $\phi = 90°$.

a basis set expansion of the induced density. This method allows one to treat more realistic models of the slab with little additional computational effort, and we have been able to determine the mode frequencies as a function of q for various orientations of the applied magnetic field. In most respects, our results are very similar to those found by Dempsey and Halperin.[28] It is therefore clear that the overall qualitative features of the dynamics is not strongly influenced by the nature of the density profile, although details of the mode dispersion are certainly modified. The main reason for the agreement between the two calculations is that both allow for the center of mass oscillation of the electron slab within the confining parabolic potential. In the work of Dempsey and Halperin this is achieved by a careful treatment of the hydrodynamic boundary conditions, while in our work it follows from a consistent treatment of the equilibrium and dynamic properties. As emphasized repeatedly, this is an essential prerequisite for the satisfaction of the generalized Kohn theorem.

The TFDW hydrodynamics we have developed can also be applied to other physical situations. Of particular interest are quantum-dot[45] and antidot[46] arrays which have recently been investigated experimentally. The collective excitations in these systems exhibit dispersions with magnetic field which are still not fully understood. It is hoped that TFDW hydrodynamics will prove useful in explaining some of this interesting behavior.

ACKNOWLEDGMENTS

[1]F. Bloch, Z. Phys. **81**, 363 (1933).

[2]G. Barton, Rep. Prog. Phys. **42**, 963 (1979).

[3]S. Lundqvist, in *Theory of the Inhomogeneous Electron Gas*, edited by S. Lundqvist and N. H. March (Plenum, New York, 1983), p. 149.

[4]F. Forstmann and R. R. Gerhardts, *Metal Optics Near the Plasma Frequency* (Springer-Verlag, Berlin, 1986).

[5]A. Eguiluz, S. C. Ying, and J. J. Quinn, Phys. Rev. B **11**, 2118 (1975).

[6]P. Hohenberg and W. Kohn, Phys. Rev. **136**, B964 (1964).

[7]A. L. Fetter and J. D. Walecka, *Quantum Theory of Many-Particle Systems* (McGraw-Hill, New York, 1971).

[8]P. C. Martin, in *Many-Body Physics,* edited by C. De Witt and R. Balian (Gordon and Breach, New York, 1968).

[9]A. D. Boardman, in *Electromagnetic Surface Modes,* edited by A. D. Boardman (Wiley, New York, 1982), p. 1.

[10]A. J. Bennett, Phys. Rev. B **1**, 203 (1970).

[11]A. D. Boardman, B. V. Paranjape, and R. Teshima, Surf. Sci. **49**, 275 (1975).

[12]C. Schwartz and W. L. Schaich, Phys. Rev. B **26**, 7008 (1982).

[13]J. E. Sipe, V. C. Y. So, M. Fukui, and G. I. Stegeman, Phys. Rev. B **21**, 4389 (1980).

[14]M. Corvi and W. L. Schaich, Phys. Rev. B **33**, 3688 (1986).

[15]V. Cataudella and V. M. Ramaglia, Phys. Rev. B **38**, 1828 (1988).

[16]U. Wulf, E. Zeeb, P. Gies, R. R. Gerhardts, and W. Hanke, Phys. Rev. B **42**, 7637 (1990).

[17]W. Kohn and L. J. Sham, Phys. Rev. **140**, A1133 (1965).

[18]T. Ando, Solid State Commun. **21**, 133 (1977).

[19]A. Zangwill and P. Soven, Phys. Rev. A **21**, 1561 (1980).

[20]M. J. Stott and E. Zaremba, Phys. Rev. A **21**, 12 (1980); **22**, 2293 (1980).

[21]K. Sturm, E. Zaremba, and K. Nuroh, Phys. Rev. B **42**, 6973 (1990).

[22]L. H. Thomas, Proc. Cambridge Philos. Soc. **23**, 542 (1926).

[23]E. Fermi, Rend. Acad. Naz. Lincei **6**, 602 (1927).

[24]C. F. von Weizsäcker, Z. Phys. **96**, 431 (1935).

[25]N. H. March, in *Theory of the Inhomogeneous Gas,* edited by S. Lundqvist and N. H. March (Plenum, New York, 1983), p. 1.

[26]M. Sundaram, A. C. Gossard, J. H. English, and R. M. Westervelt, Superlatt. Microstruct. **4**, 683 (1988).

[27]M. Shayegan, T. Sajoto, M. Santos, and C. Silvestre, Appl. Phys. Lett. **53**, 791 (1988).

[28]J. Dempsey and B. I. Halperin, Phys. Rev. B **45**, 1719 (1992).

[29]L. Brey, N. F. Johnson, and B. I. Halperin, Phys. Rev. B **40**, 10 647 (1989).

[30]Y. Tomishima and K. Yonei, J. Phys. Soc. Jpn. **21**, 142 (1966).

[31]W. Stich, E. K. U. Gross, P. Malzacher, and R. M. Dreizler, Z. Phys. A **309**, 5 (1982).

[32]A. Chizmeshya and E. Zaremba, Phys. Rev. B **37**, 2805 (1988).

[33]J. F. Dobson (unpublished).

[34]A. J. Rimberg and R. M. Westervelt, Phys. Rev. B **40**, 3970 (1989).

[35]L. Brey, J. Dempsey, N. F. Johnson, and B. I. Halperin, Phys. Rev. B **42**, 1240 (1990).

[36]T. Ando, A. B. Fowler, and F. Stern, Rev. Mod. Phys. **54**, 437 (1982).

[37]W. H. Press, B. P. Flannery, S. A. Teukolsky, and W. T. Vetterling, *Numerical Recipes* (Cambridge University Press, Cambridge, 1986).

[38]A. L. Fetter, Phys. Rev. B **32**, 7676 (1985).

[39]K. Karraï, H. D. Drew, M. W. Lee, and M. Shayegan, Phys. Rev. B **39**, 1426 (1989).

[40]K. Karraï, X. Ying, H. D. Drew, and M. Shayegan, Phys. Rev. B **40**, 12 020 (1989).

[41]K. Karraï, X. Ying, H. D. Drew, M. Santos, and M. Shayegan, in *Proceedings of the 20th International Conference on the Physics of Semiconductors,* edited by E. M. Anastassakis and J. D. Joannopoulos (World Scientific, Singapore, 1990), p. 1278.

[42]A. Wixforth, M. Sundaram, J. H. English, and A. C. Gossard, in *Proceedings of the 20th International Conference on the Physics of Semiconductors* (Ref. 41), p. 1705.

[43]A. Wixforth, M. Sundaram, K. Ensslin, J. H. English, and A. C. Gossard, Phys. Rev. B **43**, 10 000 (1991).

[44]H. A. Bethe, *Intermediate Quantum Mechanics* (Benjamin, New York, 1964).

[45]T. Demel, D. Heitmann, P. Grambow, and K. Ploog, Phys. Rev. Lett. **64**, 788 (1990).

[46]K. Kern, D. Heitmann, P. Grambow, Y. H. Zhang, and K. Ploog, Phys. Rev. Lett. **66**, 1618 (1991).